Correlations of the Evolution of a CCOPE Squall Line with Surface Thermodynamics and Kinematic Fields

Xu Yumao(徐玉貌)
Department of Atmospheric Sciences, Nanjing University, Nanjing
and *J.C. Fankhauser*
National Center for Atmospheric Research P.O. Box 3000, Boulder,
Colorado 80307 U.S.A.
Received February 8, 1988

ABSTRACT

A midlatitude squall line passed over the array of the Cooperative Convective Precipitation Experiment (CCOPE) on 1 August 1981. The structure and evolution of the squall line, and the correlations of the storm with surface thermodynamics and kinematic fields are investigated, mainly by using radar and surface mesonet data in CCOPE. The storm-wide precipitation efficiency is also estimated.

The squall line was of an obvious process of metabolism. Thirty-four cells formed successively in front of the primary storm and eventually merged into it during the period 1700-2010 MDT. The newest cells formed near surface equivalent potential temperature maxima, and near surface moisture flux convergence zones or / and the "temperature break lines". The thunderstorm rainfall, with the precipitation efficiency of 54%, lags 25-30 min behind the moisture flux convergence on the average.

I. INTRODUCTION

The structure of middle-latitude squall lines have been of considerable interest in recent two decades. Newton(1967) proposed that squall lines propagate by a combination of translation and discrete propagation of cells based on the first detailed study of the structure of a severe Oklahoma squall line. Lilly(1979), Houze and Hobbs(1982) have reviewed the current knowledge of the structure and dynamics of squall lines. Case studies(e.g., Ogura and Lion, 1980; Zipser and Matejka, 1981; Kessinger et al., 1982; Heymsfield and Schotz,1985) have revealed several fundamental features, which include intense convection at the leading edge of the squall line, gust fronts associated with downdraft outflows and cell propagation mechanisms.

A number of two-and three-dimensional numerical models of moist convection have been developed since 1980s. Thorpe, Miller and Moncrieff (1982; hereafter TMM) approached a model of mid-latitude squall lines in non-constant shear. Rotunno, Klemp and Weisman (1988; hereafter RKW) studied the mechanics of squall lines by using two-and three-dimensional numerical models of moist convection.

Many results on the correlation between boundary layer (or surface) convergence and convective precipitation have been obtained (Ulanski and Garstans, 1978; Doneaud et al., 1983; Achtermeier, 1983; Watson and Blanchard, 1984). A phase-shifted relationship

typically exists where a significant increase in convergence precedes the onset of surface rainfall and a rainfall peak lags a convergence maximum by the periods of 20 to 90 min.

The research on the impact of moist air on convective precipitation is not abundant. However, many researchers (Braham, 1952; Newton, 1966; Auer and Marwitz, 1968; Foote and Fankhauser, 1973; Fankhauser, 1982; Carbone, 1982) have estimated the inflow and precipitation efficiencies of thunderstorms and squall lines.

This study, based on a squall line that appeared near a stationary front in eastern Montana on 1 August 1981, has two purposes: (1) to investigate the correlations between the positions of new cellular development and surface thermodynamic and kinematic fields and to determine how development patterns influence and storm's overall evolution and (2) to examine the relationship between time-evolving surface moisture flux convergence and radar-derived rainfall production and to estimate the storm-wide precipitation efficiency.

II. SOURCE OF DATA AND METHOD OF ANALYSIS

Carefully calibrated and quality controlled surface mesonet and radar data from CCOPE are used in this study. A series of constant altitude contoured reflectivities at the 5 km level with 2-3 min sample interval are plotted to analyze the development and evolutions of the storm because new cells usually form at the 5-7 km level first.

The CCOPE mesonet consists of 125 sites distributed within a rectangular region having dimensions of 180 km (north-south) and 150 km (east-west) with its western border nearly centered Miles City, Montana. The average spacing between surface sites is 20 km, except for an interior region (80x80 km) with somewhat greater station density. An objective analysis scheme developed by Barnes (1973), and numerical interpolation routines by Mohr et al. (1981) are used on data which are recorded at 5-min intervals to obtain horizontal contour fields of wind (streamlines, divergence), equivalent potential temperatures (θ_e) mixing ratios (q) and moisture flux convergences ($\rho\nabla \cdot q\bar{v}$). Ancillary data from cloud base aircraft and multiple Doppler radar synthesis are also available during a short period of the squall lines history.

In order to investigate the corresponding relation in time and space between radar echoes and surface mososcale fields, we define a moving window of constant size (80x80 km) which encircles the active part of the storm for both echoes and surface analyses.

III. GENERAL SYNOPSIS

The storms formed in the afternoon on 1 August 1981 in eastern Montana. At 1800 MDT, the mesonet in CCOPE lay in the west-southwest flow between two troughs at levels higher than 700 hPa and northeast of a depression at 850 hPa. The surface chart analysis shows a weak stationary front passed through Miles City during 1500 MDT 1 August to 1800 MDT 2 August.

Temperature and dewpoint profiles from a sounding at Miles City (MLS) are shown in Fig. 1. Combining the subcloud aircraft and MLS sounding data, we obtain the lifting condensation level (H_L) of 685 hPa (3342 m) and the free convection level (H_F) of 652 hPa (3753 m) and Showalter index of −4.6, respectively. The air over MLS was possessed of potential instability stratification with rather large instability energy.

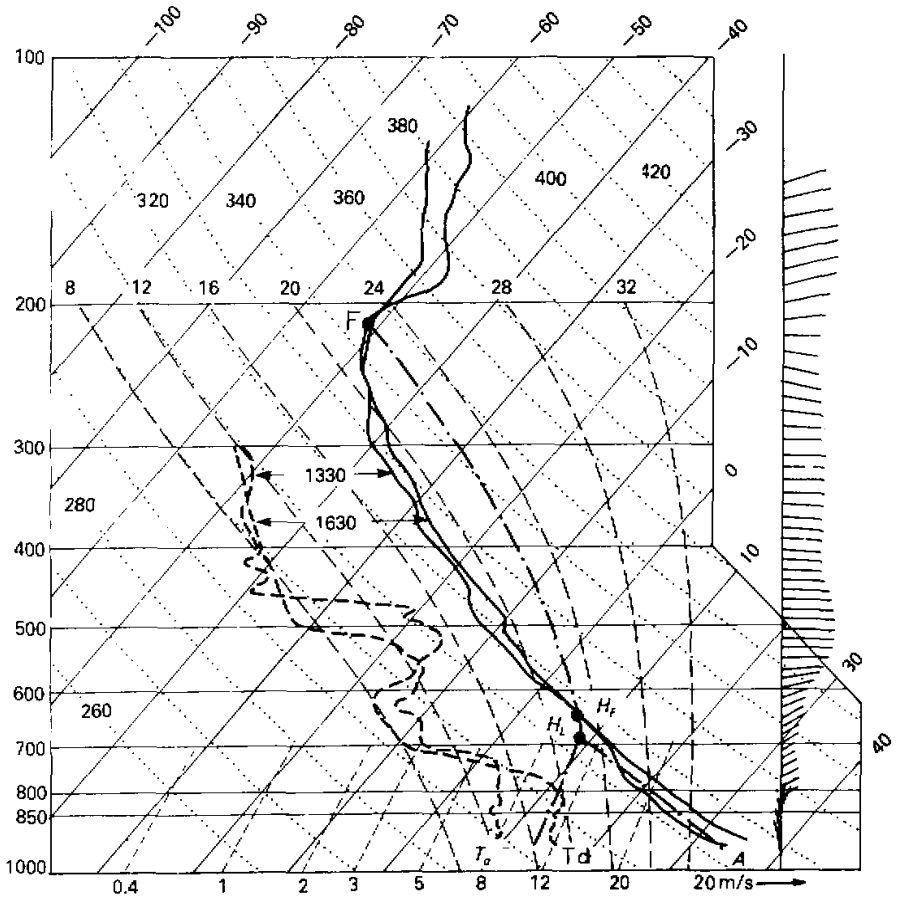

Fig.1. Tephigram showing temperature (T, solid lines) and dew point (T_d, dashed lines) for MLS sounding at 1330 and 1630 MDT and aircraft measurement at 1730–1750 MDT (dot–dashed line) with wind vectors on the right.

Wind vectors on the right of Fig.1 show the presence of a stronger shear between surface and middle level. It is a favorable condition for long–lived convection of a squall line (TMM, 1982; RKW,1988).

IV. EVOLUTION OF RADAR ECHO

1. *Generalization*

The squall line passed through the CCOPE array from 1640 to 2030 MDT on 1 August. The development of echoes from 1700 to 2000 MDT is shown in Fig.2. The large echo A (called host echo) in the north is a multicellular echo. Four cells (reflectivity factor $Z \geq 40$ dBZ) are clearly seen at 1702 MDT. We call the new cells formed in front of echo A cell C_1 , C_2 ,... C_n beginning from 1701 MDT. The host echo A moved southeastward at an average speed of 310 ° / 15 ms^{-1}. The new cells in front of A were

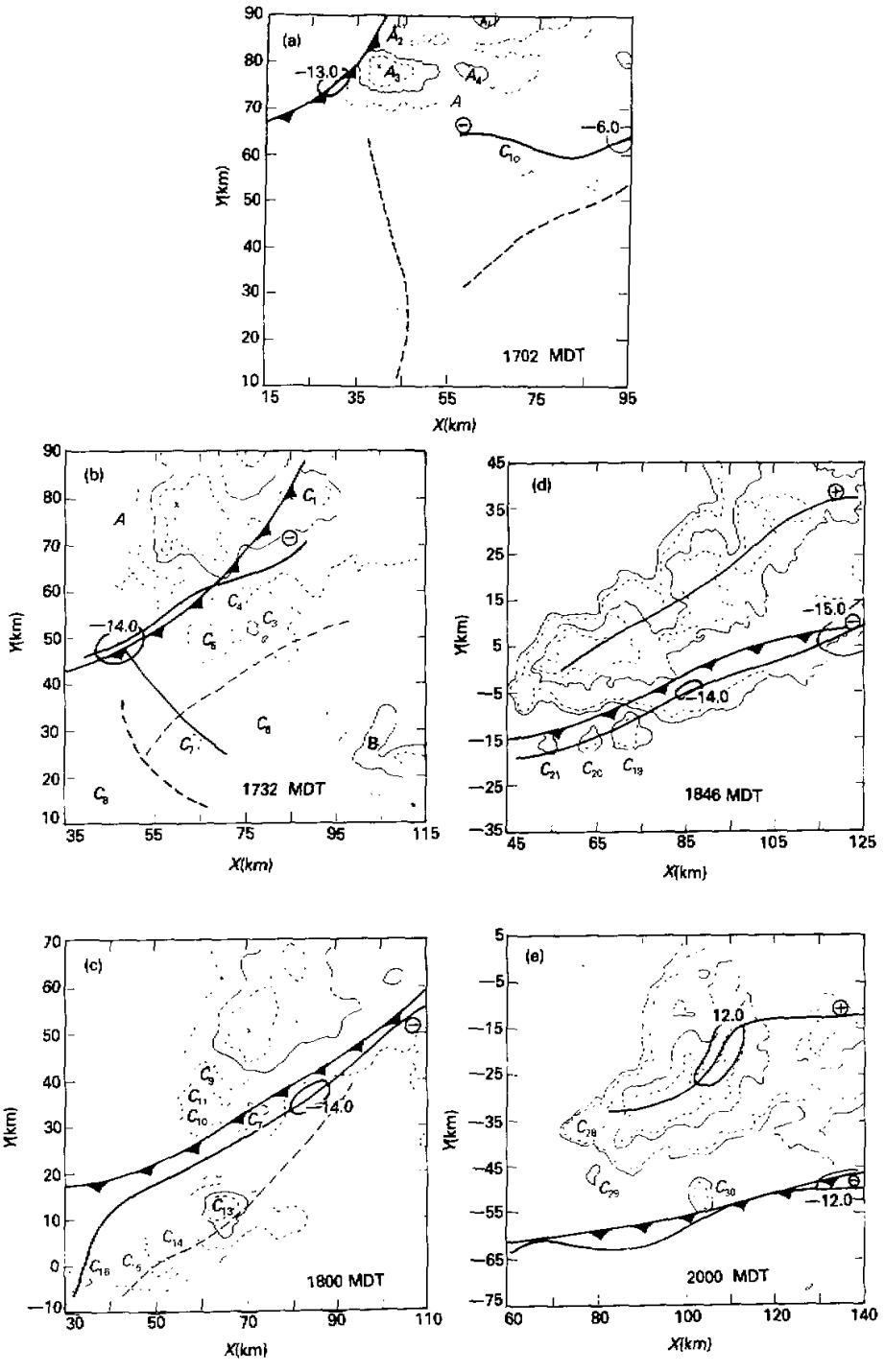
(a)
1702 MDT
(b)
1732 MDT
(c)
1800 MDT
(d)
1846 MDT
(e)
2000 MDT
Y(km)
X(km)

Fig.2. Developments of echoes on CAPPI of 5 km level. Numbers in center of reflectivity contours (10, 20, 30,..... dBZ) show numbers of new cells. Additionally, dashed lines are θ_s axes; solid lines and circles are QFLUX axes and the extreme value areas (symbols ⊕ and ⊖ represent $QFLUX_+$ and $QFLUX_-$); barbed fronts are temperature break lines.

very active andcontinuously merged into A after they appeared. For example, cells C_1–C_5 merged into A before and after the time interval of 1701–1732 (Fig. 2b) and echo B amalgamated with A after 1747 MDT. During 1703–1759 (Fig. 2c) four new cells formed in succession to the southwest of the main echo complex and then joined with A at about 1817. After that, the host echo A was sustained and evolved through merging of new cells that formed primarily on the southwestern sector as the complex as a whole moved southeastward (Figs. 2d–e). The rain stopped before 2100 MDT.

2. *Activities of the New Cells*

Fig. 3a illustrates the formation and joint procedure of new cells. The A represents the host echoes as defined in Section 1. C_1 , C_2 ,... C_{34} are new cells formed at successive times. The horizontal solid lines, including the bold lines, show the life periods of each new cell. The bold lines indicate which cell has the highest reflectivity at time t and the duration of its Z_{max} core.

Fig.3 reveals the following facts: 1) 34 cells formed in front of and / or adjacent to the host echo A and eventually merged into A in the period 1700–2010 MDT; 2) The new cells occurr at different frequencies with the maximum speed of 1 cell per 2 min, the minimum of 1 cell per 21 min, and the average frequency is 1 cell per 5.5 min. the result is consistent with one every 5 min found in an Alberta hailstorm analyzed by Renick (1971); 3) The new cells can be classified into five groups. It is shown by comparing Fig.3a with Fig.3b that joining of each group of new cells with echo A responds to a peak in the maximum radar reflectivity (middle curve in Fig.3b) and areal echo coverage for intensity of $\geq$25dBZ (top curve) and 45 dBZ (bottom curve), with a phase separation of 20 to 50 minutes. It demonstrates that the formation and merging of new cells with the host echo play a role in invigorating and maintaining the host echo; 4) In the development process of multicellular thunderstorms, the position of Z_{max} is moving towards the new echoes in turn which has grown stronger. The strongest echo core located in the primary host echo at the earlier stage. From about 1830, the highest reflectivities are found in C_{14} and C_{17} (i.e. the position where the third group of new cells join up with A as they get mature, and then move to the location of the fourth and fifth groups. This behavior shows clearly the process of metabolism of multicell storm.

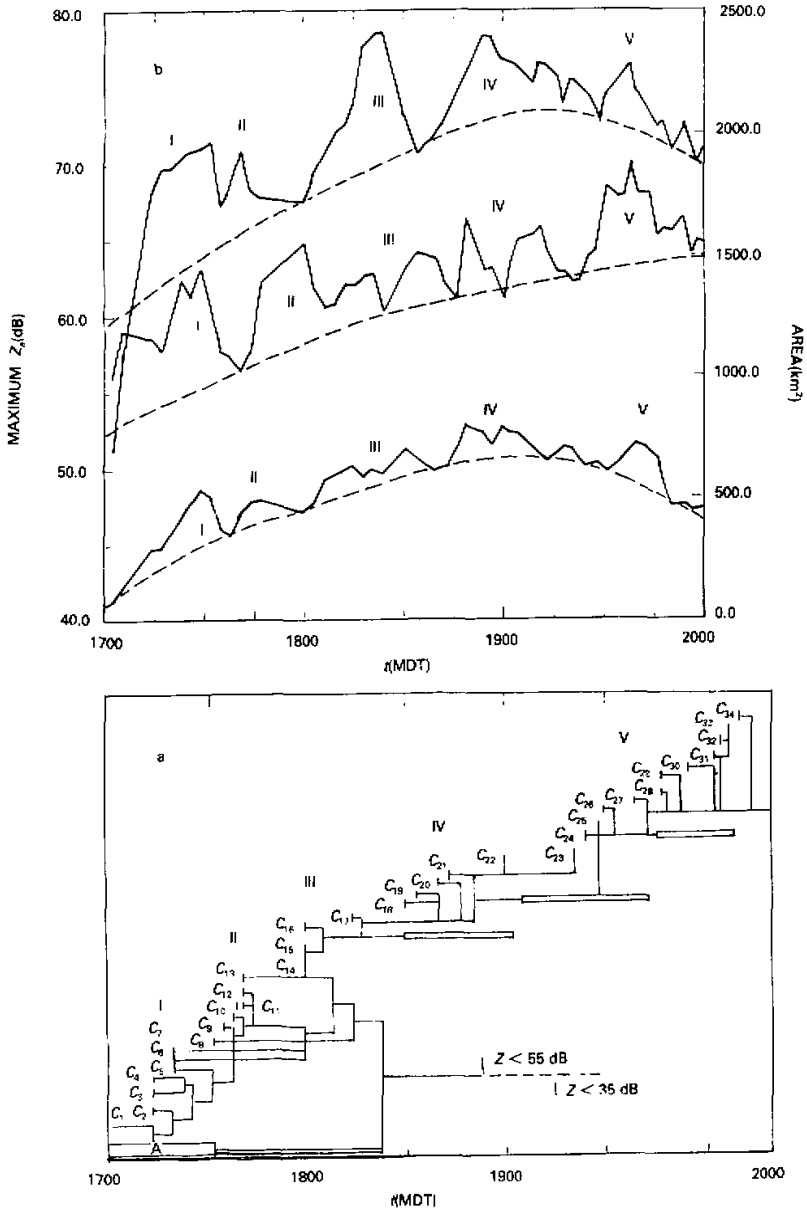

Fig.3. (a) History of cellular development. (b) temporal profile of maximum Ze (middle line), echo area for intensity of $\geq$ 25dBZ (top curve) and 45 dBZ (bottom curve).

V. CORRELATION BETWEEN EVOLUTION OF STORM AND SURFACE THERMODYNAMICS AND KINEMATIC FIELDS

Fig.2 shows the newest cells formed near surface equivalent potential temperature (θ_e) maxima, the moisture flux convergence (i.e. QFLUX_) zones and near the temperature break lines.

In order to obtain the correlations between the positions of new cellular development and surface fields, and how the development patterns influence the storm's overall evolution in detail, Fig. 4 and Fig.5 are drawn. According to Fig. 5a, all new cells form in the moisture flux convergence (QFLUX_) regions except C_{13} and C_{23} . Before 1730 MDT there is a QFLUX_ axis located in warm air southeast of the break line marking the outflow from echo A . However, after 1730 MDT the QFLUX_ axis are close to the outflow boundary and remain nearly parallel thereafter (Fig.2). The temperature break lines correspond to the surface gust front position and represent the interface between outflow caused by downdraft and the inflow in front of it. From 1845 on, a QFLUX$_+$ (moisture flux divergence) axis develops beneath the high reflectivity region paralleling to the break line associated with QFLUX_ axis (Fig.2d–e). It shows that the prevailing downdraft casued by precipitation at the rear part of the cloud led to surface moisture flux divergence at the mature stage. This is also demonstrated by mesoscale streamline analysis in Fig.5. Figure 4 shows that most new cells appeared in the convergence regions ahead of the break line prior to 1830 MDT, but the cells occurred in the convergence area on or behind the break line after 1831 MDT. This convergence area on the front–right side of the host echo resulted from the fact that the divergent flow from the core of the host echo increased the convergence at the gust front boundary after 1830 (Fig. 5c–e). It shows that the downdraft produced by precipitation can enhance and / or help maintain an original convergence line.

Figure 4b indicates that at the beginning the new cells are farther away from the break line, at the maximum distance of 40 km and then they become closer gradually, and the new cells form at a distance of 14 km behind the break line after 1830 MDT. It could be explained as follows: the break line moves faster than the echo system does. The break line moves out from beneath the host echo originally. After 1900 MDT, it moves to the front of the echo system (Fig.2). It means that the downdraft runs faster and extends wider (farther). Hence, the ascending current lifted by the break line would form clouds behind the break line. The data from Doppler radar show that the new cells form in the ascending current area on the front–right side of the host echo although they lie behind the break line (Figure not shown). The analysis from cloud base aircraft data presents that the new cells C_{21} at 1845 MDT is homogeneous with the area of vertical speed of 3 ms^{-1} and C_{24} at 1905 MDT coincides with the ascending air area with the maximum speed of 9 m s^{-1} (Fig.6).

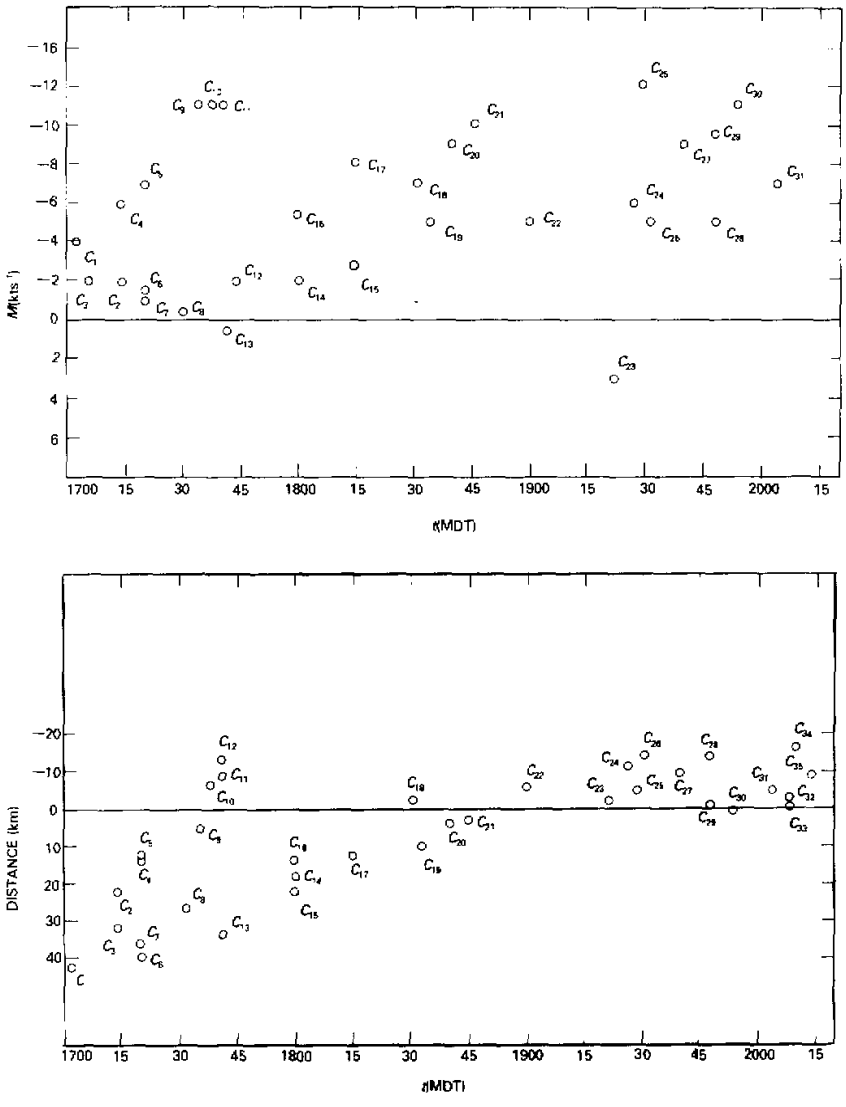

Fig.4. Relationships in time and space of new cells (Ci) with surface moisture flux divergence (M) and temperature break line. (a) M values related to new cells. Abscissa denotes the time (MDT), ordinate is M values. The negative M denotes moisture flux convergence; (b) Distances between Ci and temperature break lines (positive value shows that Ci locates in front of or on the right of break line).

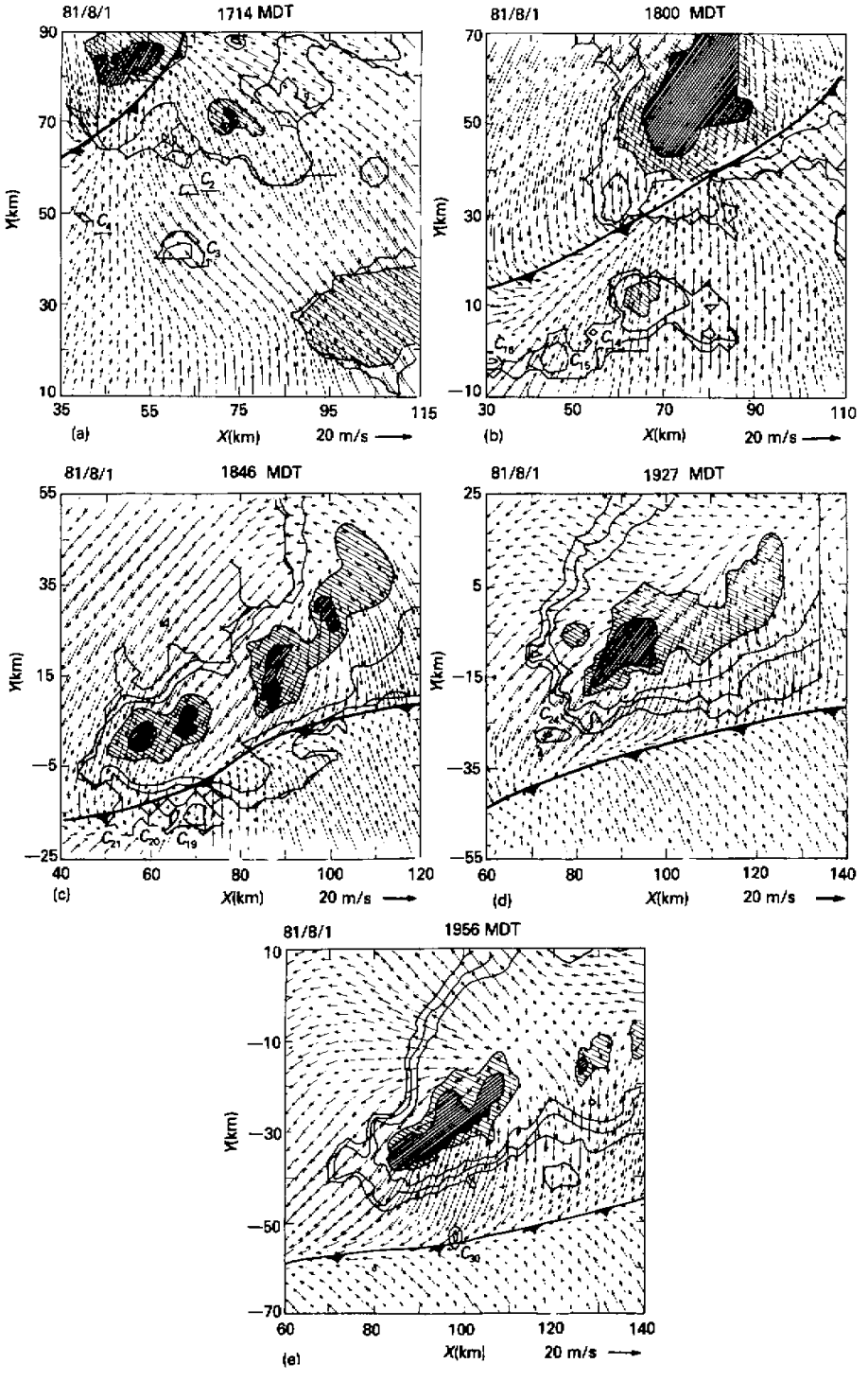
81/8/1 1714 MDT
81/8/1 1800 MDT
81/8/1 1846 MDT
81/8/1 1927 MDT
81/8/1 1956 MDT
Y(km)
X(km)
20 m/s
(a)
(b)
(c)
(d)
(e)

Fig.5. Meso-analysis of surface streamlines and echo contours of 5, 15, 25, 45, and 55 dBZ on CAPPI of 5 km. Barbed front and Ci are the same as those in Fig.2.

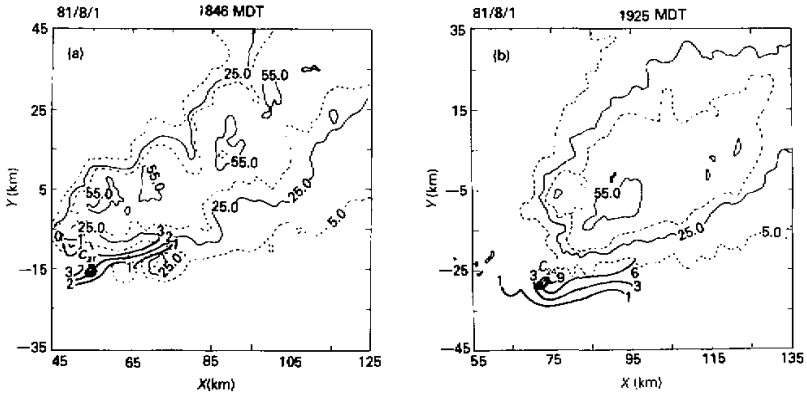

Fig.6. Vertical velocities (ms^{-1}, bold curves) from aircraft measurement at cloud base attached to radar echoes.

In summary, the foregoing analysis illustrates the following:

1. The high θ_e area provides the formation of convective cloud with instability conditions;

2. The surface moisture flux convergence line (or zone) during the formation stage of the storm, which includes two factors for forming cloud and precipitation—vertical ascending motion and moisture, and / or the break line are a triggering mechanism of the formation of echoes;

3. The moisture flux divergence line (QFLUX$_2$ axis) is the result of precipitation. However, it exerts a feedback effect on the formation of echoes. That is, the downdraft caused by rainfall from the beginning of the mature stage can invigorate and keep the original convergence line (QFLUX$_1$ axis), which impels the formation of new cells on the front-right side of the host echo system.

VI. MOISTURE FLUX CONVERGENCE AND PRECIPITATION EFFICIENCY

As has been stated, the surface moisture flux convergence is a triggering mechanism of cloud and precipitation. In fact it is a moisture source of cloud and rainfall. As a result it affects the precipitation efficiency. A radar reflectivity (Ze) versus rain rate (R) relationship is used to estimate the thunderstorm rainout since raingauge data in this case are not sufficient enough to calculate the precipitation produced by the whole storm. According to Fankhauser's study (1986), the surface moisture flux convergences are very close to the cloud base flux. Therefore, we define the precipitation efficiency (η) as a ratio of rainout derived from radar reflectivity at 5 km level to moisture flux convergence in the subcloud layer.

It is necessary to adapt a Z–R relation appropriate for the experimental extent in order

to optimize the estimates of the storm's rainout. We have used data from seven raingauges in the experimental region and the Ze values in the corresponding periods and spaces (i.e.the average Ze in the (2x2x2) km^3box at the 3–5 km level over the raingauges) to obtain the Z–R relation. The result is as follows:

$$Z = 922R^{1.28}. \tag{1}$$

The areally–averaged surface rainfall at time t, $P(t)$, from radar–estimated rainrate(R) by using formula (1), may be obtained

$$P(t) = \int_A R(t)dA, \tag{2}$$

where A is the area of the analysis' window.

The areally–integrated surface moisture flux at t on the same window is computed from

$$M(t) = \rho\int_A \nabla\cdot q\bar{v}(t)dAdz, \tag{3}$$

where dz is the subcloud layer depth.

Figure 7 gives the temporal profiles of the areally integrated moisture flux convergence (dashed curve) and the thunderstorm water mass rainout (solid curve). The moisture flux convergence during 1400–1700 MDT is plotted into the figure. It is seen that a significant increase in convergence precedes the onset of surface rainfall, and a phase shifted relation between M and P. It is difficult to estimate the precipitation efficiencies at different times because of the complicated variation of M and P with time here. However, we have determined their phase relation (the numbers in Fig.7 represent the relevant wave crests) according to the shapes of the wavelike curves in the figure and the estimation of the time required for an air parcel ascended up to the cloud from surface. The phase–lags between P and M are shown in Table 1. The thunderstorm rainout lags 27.4 min. behind the water vapor inflow on the average.

The second method to determine the phase–lag between rainout and moisture flux convergence is gained from the corresponding relation between maximum Ze and minimum QFLUX_. Table 2 gives the times that maximum reflectivities lag behind the corresponding minimum QFLUX_ in space position. Maximum Ze is formed 27.1 min after minimum QFLUX_ appears, which is surprisingly consistent with the result (27.4 min) obtained by the first method.

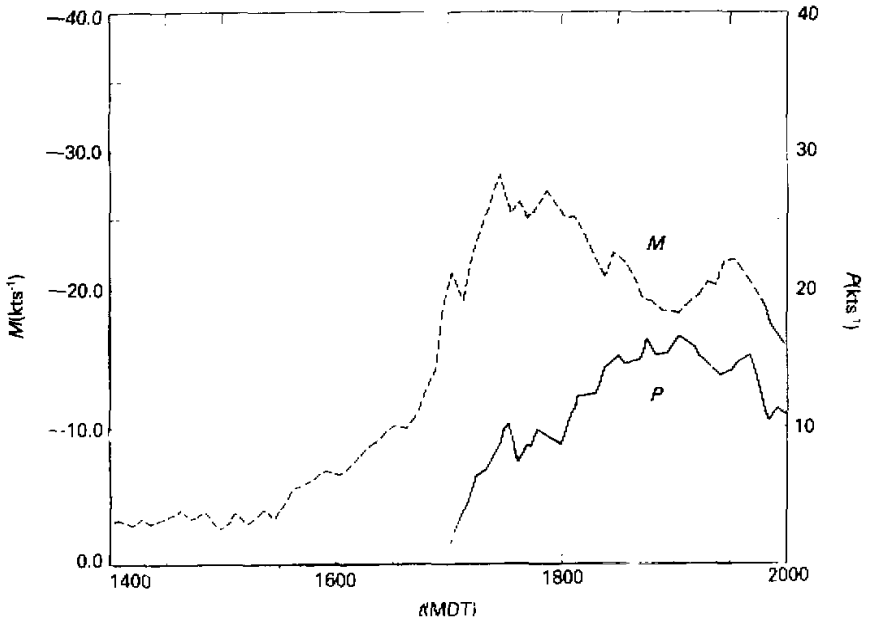

Fig.7. Temporal profiles of thunderstorm water mass rainout (solid curve), and the subcloud layer moisture flux convergence (dashed curve). Units of abscissa are kiloton per second (kts^{-1}).

Table 1. Phase–Lags (Δt) between P and M and Precipitation Efficiencies (η)

t (MDT)	1730	1745	1830	1900	1940	
Δt (min)	30	20	39	35	13	t=27.4
η (%)	48	36	56	74	70	

Table 2. Phase–Lags between Maximum Ze and Minimum $QFLUX$

t (min $M-$)	1657	1702	1707	1712	1717	1722	1727	1732	1737	1737
t (max Ze)	1726	1735	1738	1741	1741	1744	1700	1760	1760	1806
Δt (min)	29	33	31	29	24	22	33	28	23	29
t (min $M-$)	1752	1752	1757	1757	1807	1827	1847	1917	1927	1932
t (max Ze)	1815	1818	1815	1818	1831	1854	1916	1946	1956	2004
Δt (min)	23	26	18	21	24	27	29	32	29	32
Δt (min)				27.1						

The result shown above is the same as that indicated by Byers and Braham (1949) – surface convergence is detectable 20–30 min before the radar echo appears. It is a bit shorter than the 35–min period obtained by Watson and Blanchard (1984) in the Florida Cumulus

Experiment.

Table 1 shows that the variation of precipitation efficiency (η) with time is not homogeneous. η is smaller at the earlier stage, but it rises at the development stage and reaches the largest value at 1900 MDT, then begins to drop once more. It seems to reflect the development process— " rainmaking" and "rainfall" process, i.e., " water-storing " and "water-drawing" processes in the multicell thunderstorm cloud. But it also may be due to the variation of environment conditions with time, or the uncertainty of observations and analysis. Therefore, it is necessary to do further research for other cases.

The storm-wide precipitation efficiency during 1700–2000 MDT, obtained dividing the rain water mass deposited between 1700 and 2000 MDT by the corresponding vertical water vapor flux from surface to cloud base is 54%, quite comparable to those reported earlier for other squall lines.

VII. SUMMARY AND CONCLUSION

The study of a CCOPE squall line here confirms and complements the features of midlatitude squall line. The squall line composed of multicellular thunderstorm has an obvious process of metabolism, which belongs to the first type of long-lived squall lines simulated by RRW (1988): a line of more or less ordinary cumulonimbi with unsteady cells growing and decaying. The evolution of the storm is in close relationship with surface thermodynamics and kinematic fields. The newest cells formed near surface equivalent potential temperature (θ_e) maxima, which consist with the results of all case studies that the cumulonimbi composed of the line are fed by the low-level high θ_e air ahead of the line. The new cells formed near surface moisture flux convergence zone which provides the water vapor and the ascending motion for the formation of echoes and near surface "temperature break lines" at the leading edge of the cold air outflow caused by heavy rain near the back of the cloud line. The cold air outflow will, in turn, enhance the moisture flux convergence and will impel the formation of waves of new cells.

The phase lag between the areally integrated moisture flux convergence and rainfall is 25–30 minutes on the average, which is consistent with the typical lifetime of an individual thunderstorm cell as first defined by Byers and Braham (1949). The storm-wide precipitation efficiency is different from time to time, and the average value during 1700–2000 MDT is 54%, quite comparable to those reported earlier for other squall lines.

The authors would like to express deep appreciation to L.J. Miller for his suggestion on calculation methods and to Charles G. Wade for the provision of synoptic data. Appreciation is also due to C.G. Mohr assisted in the use of the computer.

REFERENCES

Achtemeier, Gary L.(1983),The relationship between the surface wind field and convective precipitation over the St. Louis area, *J. Appl. Meteor.*, **22**: 982–999.

Barnes, S.L.(1973), Mesoscale objective map analysis using weighted time-series observations, NOAA Tech. Memo ERL NSSL-62, 60 pp.[NTISCOM-73-10781].

Byers, H.R., and R.R. Braham, Jr.(1949), The thunderstorm, U.S. Govt. Printing Office, Washington, D.C., 282 pp.

Doneaud, A.A., J.R. Miller, et al.(1983), Surface mesoscale features as potential storm predictors in the Northern Great Plains-- two case studies, *Mon. Wea. Rev.*, **111:** 273-292.

Heymsfield, G.M., and S.Schotz (1985), Structure and evolution of a severe squall line over Oklahoma, *Mon. Wea. Rev.* **113:** 1563-1589.

Houze, R.A., Jr., and P.V. Hobbs (1982), Organization and structure of precipitating cloud system, *Advances in Geophysics*, **24:** Academic Press, 225-315

Kessinger, C.J., C.E. Hane and P.S. Ray (1982), A Doppler analysis of squall line convection, Preprints, 12th Conf. Severe Local Storms, San Antonio, *Amer. Meteor. Soc.*, 123-126.

Lilly, D.K. (1979), The dynamical structure and evolution of thunderstorms and squall lines, *Annual Reviews in Earth and Planetary Sciences*, **7:** Annual Reviews, 117-161.

Mohr, C.G., L.J. Miller, and R.L. Vaughan (1981), An interactive software package for dimensional Cartesian coordinates, Preprints, 20th Conf. on Radar Meteor., *Amer. Meteor. Soc.*, Boston, 690-695.

Newton, C.W. (1967), Severe convective storms, *Advances in Geophysics*, **12:** Academic Press, 257-308.

Ogura, Y., and M.T. Liou(1980),The structure of a midlatitude squall: A case study, *J. Atmos. Sci.*, **37:** 553-567.

Renick, J.H. (1971), Radar reflectivity profiles of individual cells in a persistent multicellular Alberta hailstorm, Preprints, 7th Conf. Severe Local Storms, *Amer. Meteor. Soc.*, Boston, 63-70.

Rotunno, R., J.B. Klemp and M.L. Weisman(1988),A theory for squall lines, *J. Atmos. Sci.*, (be published soon).

Thorpe, A.J., M.J. Miller and M.W. Moncrieff(1982), Two-dimensional convection in non-constant shear: a model of mid-latitude squall lines, *Quart. J.Roy. Meteor. Soc.*, **108:** 739-762.

Ulanski, S.L., and M. Garstang(1978), The role of surface divergence and vorticity in the life cycle of convective rainfall. Part I: Observation and analysis, *J. Atmos. Sci.*, **35:** 1007-1062.

Watson, A.I., and D.O. Blanchard (1984), The relationship between total area divergence and convective precipitation in South Florida, *Mon. Wea. Rev.*, **112:** 673-685.

Zipser, E.J.,and T.J. Matejka(1981), Comparison of radar and wind cross-sections through a tropical and a midwestern squall line, Preprints, 12th Conf. Severe Local Storms, San Antonio, *Amer. Meteor. Soc.*, 342-345.